Multicycle Flash Sintering of Cubic Y_2O_3-stabilized ZrO_2: An *in situ* energy dispersive synchrotron x-ray diffraction study with high temporal resolution

Hülya Biçer[1], Ahmed Degnah[2,*], Emin Salur[3], İlyas Şavklıyıldız[4] Thomas Tsakalakos[5], E. Koray Akdoğan[5]

[1]Department of Metallurgy and Materials Engineering, Kütahya Dumlupınar University, Kütahya, 43000 Turkey.

[2]National Center for Advanced Materials Technologies, King Abdulaziz City for Science and Technology (KACST), P.O Box 6086, Riyadh 11442, Saudi Arabia

[3]Department of Metallurgical and Materials Engineering, Selçuk University, Konya, 42075, Turkey

[4]Department of Metallurgy and Materials Engineering, Konya Teknik University, Konya, 42075 Turkey.

[5]Department of Materials Science & Engineering, Rutgers University, Piscataway, New Jersey 08904, USA.

***Corresponding Author's E-mail:** adegnah@kacst.edu.sa
***Corresponding Author's Address:** National Center for Advanced Materials Technologies, King Abdulaziz City for Science and Technology (KACST), P.O Box 6086, Riyadh 11442, Saudi Arabia; Phone: + 966 1 4883555 Ext: 4128

Abstract

The current induced unit cell volume changes, (111) Bragg peak full width at half maximum (FWHM) and its integrated intensity in 8% Y_2O_3 stabilized ZrO_2 (8%YSZ) solid state electrolyte was monitored during a triple-flash sintering experiment by *in situ* energy dispersive x-ray diffraction using a polychromatic synchrotron probe (max, photon energy 200 keV) with 2 second temporal resolution. The first spontaneous singularity in the unit cell volume (+0.54%) was observed at 899 ^oC under 15 V/mm applied field intensity, which was associated with 13 mA/mm^2 current draw and an increase in density to 97%. Following anelastic relaxation of the unit cell volume under open circuit conditions, the same applied field was applied twice in a row which resulted in additional induced singularities at 925 ^oC (+0.48%) and 944 ^oC (+0.42%). A floating baseline, which was above the thermal expansion baseline, was observed from 833-969 ^oC and was attributed to Joule heating. The singularity at 899 ^oC is associated with a sharp change in (111) FWHM and a 34% decrease in integrated peak area that was attributed to changes in the distribution of oxygen vacancies and the changes in their concentration as induced by the applied field in the spontaneous transient stage of flash sintering.

Keywords: Flash sintering, energy dispersive x-ray diffraction, synchrotron diffraction, lattice expansion, diffusion.

I. Introduction

Sintering of ceramics at elevated temperatures remains to be a challenging phenomenon in ceramics engineering as it relies on limited thermodynamic driving forces that arise from specific surface are of particulate matter. The kinetic side of the phenomenon is plagued with sluggish diffusion rates that is associated with ambipolar diffusion in nonmetallic and inorganic materials[1]. A variety of approaches were developed to improve the thermokinetics of the sintering process[1-4]. Flash sintering is one of the electric field-assisted sintering techniques that reduces densification temperature by approximately 50%, while reducing the sintering time by approximately one to two orders of magnitude, i.e., from hours to seconds[5-13]. Cologna et al. flash sintered yttria-stabilized zirconia to 97% of theoretical density at 850°C (conventional sintering temperature is ≥1200°C) under 120V/cm electric field in as little as 5 seconds [14]. A variety of ceramic material systems have been successfully densified by flash sintering ever since [9, 11, 12, 15-17].

The flash sintering process is closely related to the temperature dependence of electrical conductivity of a give ceramic although the exact mechanisms remain to be unearthed. To date, three distinct stages in flash sintering were identified: (i) the incubation stage (open circuit condition) -the period preceding the precipitous rise in current where the specimen behaves as an insulator; (ii) the transition stage (transient closed circuit condition) -the current rises precipitously to its maximum value (cut-off) at which point the power source switches from voltage to current control; and (iii) the steady-state (closed circuit condition) where both the current and voltage are kept constant. If this stage is not avoided, grain growth is known to occur[7, 10, 18-21]. In some experiments, the third stage is completely avoided, and the power is turned off where the system assumes an open circuit condition. The

aforementioned rapid increase in the current draw by the specimen, which sets in at a temperature that is specific to the material of interest, is accompanied by precipitous densification.

Mass transport phenomena in crystalline solids is governed by the diffusion of atoms, ions, or other charged species, and the type and concentration of defects in the material of interest [7, 10, 12, 18-21]. Therefore, it is vital to understand the role of defects in flash sintering of ceramics. Specifically, 8% yttria stabilized zirconia is an ionic conductor in which the transport of oxygen vacancies constitutes the rate limiting step in mass transport in the solid state[22-28]. If ionized, such oxygen vacancies can couple with the applied electric field and provide sizeable contribution to the electrochemical potential that controls the diffusion flux[10].

Several densification mechanisms for flash sintering were proposed, including excess Joule heating and the formation of vacancy and Frenkel pairs, among many others [10, 15, 16, 21, 23, 29-35]. While Joule heating (the top contender among the proposed mechanism) cannot be ignored in flash sintering, there is an increasing amount of evidence that the ultra-rapid densification rates cannot be explained by Joule heating solely [5, 6, 11, 12]. However, no consensus has been reached regarding the mechanism that chiefly governs flash sintering. Various structural changes occurring during flash sintering were reported [27, 28, 34, 36]. Moreover, *in situ* energy dispersive synchrotron x-ray diffraction studies by the authors led to the discovery of an anomalous unit cell expansion accompanying the power absorption by the ceramic body in stage two of flash sintering[5, 6]. There are now many studies in which the use of flash sintering was successfully demonstrated for a plethora of systems, making it a universal phenomenon[18, 30].

In this study, 8 % Y_2O_3 stabilized ZrO_2 was densified by flash sintering using a multicycle approach. Specifically, we have "flashed" the specimen two more times by turning the power source on and off after the spontaneous flash had occurred. In so doing, we gained valuable insight to the "anatomy" of flash sintering thanks to the high temporal resolution x-ray diffraction method that we implemented into this multicycle flash sintering experiment.

II. Experimental

Commercial 8% Y_2O_3 stabilized Zr_2O[23, 25, 28] (8YSZ) with 200 nm median particle size was used in the study. The powder was pressed uniaxially into a 12 mm disc-shaped specimen with 2.7 mm thickness. The density of the as-pressed specimen was %55 of the theoretical density.

The energy dispersive x-ray diffraction (EDXRD) work in this study was carried out in the National Synchrotron Light Source (NSLS) at Brookhaven National Laboratory (BNL), Upton, New York. High photon energy (up to 200 keV) used with ultrahigh EDXRD enables the data collection from the body center of the material with high temporal resolution [37, 38]. The diffraction technique used in this study is a transmission method in which the specimen is stationary. Here, high energy polychromatic incident photons scatter at a fixed Bragg angle (θ=1.5° in this study), and a germanium detector is used to collect the data. Diffraction volume (known as the gauge volume; GV) is fixed in space the volume of which is controlled by the diffraction optics which is variable. The GV used in this study is over ~25 mm^3, ensuring good counting statistics as the particle size of equiaxed particles in the 8YSZ was 250 nm. Full x-ray spectra were collected with 2 seconds temporal

resolution. Further details of the diffraction techniques that was used in this study can be found elsewhere[39-47].

A custom-made hot stage was utilized for in-situ diffraction experiments as described in Refs.[5, 6, 38]. The specimen was placed between two insulators, and the specimen holder was heated resistively with an external power source. Platinum wire and platinum foil were used to establish ohmic contacts with the specimen to apply an electric field through a second power source. The hot stage was mounted on the x-y-z positioning stage in the beamline and the gauge volume was placed on the body center [39-47]. Fig. 1 exhibits schematics depicting the X17-B1 beamline at NSLS-BNL and the diffraction stage used for ultra-high energy energy dispersive x-ray diffractometry and the custom hot-stage used in the experiment [5].

The specimen was heated with a heating rate of (15°C/min) under the 15 V/mm electric field. The current density limit was set to 13.25 mA/mm^2 to prevent the sample from thermal runaway due to excessive Joule heating. The voltage, current, and temperature data were monitored concomitantly with the diffraction data. Once densification was completed following the transient state (precipitous rise in current density), the power source was cut off to severely limit Joule heating. After the initial power cut-off, the power was turned back on and off two more times to assess if the precipitous rise in the current and the accompanying anomalous unit cell expansion repeated itself.

The collected data were analyzed by the following equation

$$\frac{1}{d_{hkl}} = \left[\frac{2\sin(\theta)}{hc}\right] E_{hkl}\,, \quad (1)$$

where E_{hkl}'s are the diffracted energy from crystallographic planes with Miller indices (hkl), d_{hkl}'s are the interplanar spacings of the said planes, h is Plank's constant, c is the speed of light, and θ is the Bragg angle that is fixed in the experiment. Here, the $(1/d_{hkl}) = |Q_{hkl}|$, where $|Q_{hkl}|$ is the magnitude of the reciprocal lattice vector corresponding to a certain (hkl). As a consequence, the d_{hkl} data is of high accuracy

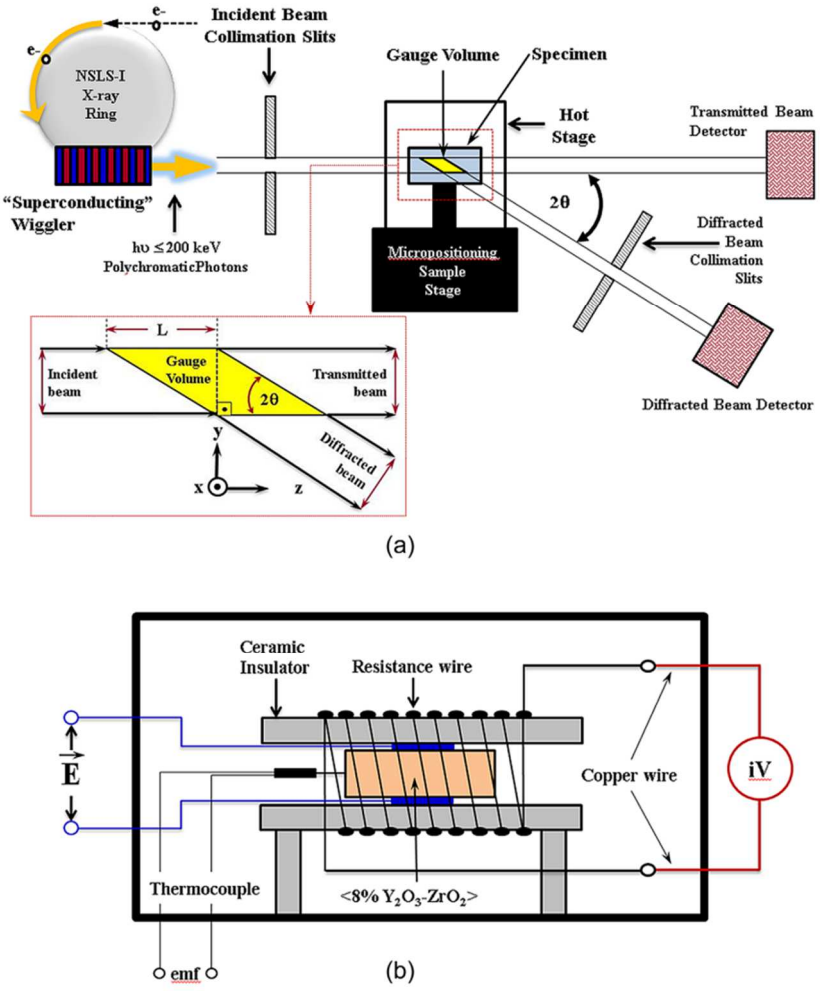

Figure 1. Schematic depicting (a) the energy dispersive X-ray diffraction set-up at BNL and (b) custom-made hot stage used in the experiment [5]

since it is obtained by the direct measurement of E_{hkl}. LaB_6 (NIST SRM660*)*, CeO_2 (NIST SRM674), and Au standards were used for the energy calibration using an in-

house protocol. A Gaussian profile shape function was employed for obtaining the position of the peak centroid and peak breadth at half maximum. The lattice parameter and unit cell volume of the cubic 8%YSZ were calculated from the (111), (200), (220), and (311) d-spacing data with the help of the UnitCell software package [48].

The densities of 8%YSZ specimens were determined by the Archimedes method. The microstructures of the specimens were analyzed with a field emission scanning electron microscope (FE-SEM, Hitachi SU 5000).

III. Results and Discussion

The variation of the current density and power dissipation as a function of time under 15 V/mm applied time invariant (dc) electric field intensity is depicted in **Fig. 2.** Up to 833 °C, no current draw from the specimen was observed, indicating that the specimen was in an insulating state due to its negligible conductivity. In other words, there was no conduction across particle-particle contacts inside the specimen. The current leakage started at 833 °C at which point its value reached 1 mA/mm^2 and lasted for the following 180 seconds (the incubation period of flash sintering in this experiment). At the end of the said incubation period the transient stage (stage two) of the flash sintering began. Here, the current rose precipitously, reaching a maximum of 13 mA/mm^2 in 75 seconds at 899 °C. The peak power density that was absorbed by the specimen in this stage was as 99.47 mW/mm^3. In other words, the specimen sintered within 75 seconds at a peak furnace temperature of 899 ^{o}C as is typical of flash sintering. Once the current reached a maximum at 899 ^{o}C, the power source was turned off to prevent excessive Joule heating. After waiting for 30 seconds, the power source was turned on while the sample was being heated

(heating was never ceased until the very end of the experiment). The current precipitously rose to again, reaching its maximum of 9.98 mA/mm^2 at 925 °C at which point the power was cut off. Again, after waiting for 30 seconds, the power source was turned on while the sample was continued to be heated. The current precipitously rose, reaching its maximum of 8.90 mA/mm^2 at 944 °C at which point the power was cut off. In other words, the current draw by the specimen decreased after the first singularity although the furnace temperature kept on increasing which should, in principle, also increase the conductivity of 8YSZ. Since the specimen undergoes densification by the end of the first current draw (hence the highest current draw among the 3 peaks in power absorption), we conclude that the formation of the grain boundaries have a correlation with the lower current draw by the specimen at 925 and 944 ^{o}C. This, in turn, suggests that the conductivity of 8%YSZ is interface controlled in flash sintered specimens. As such, we infer that the grain boundaries and the associated space charge become an impedance to charge transport. In what follows, we will analyze the correlation between the observed current-voltage behavior and the variation of the 8%YSZ cubic unit cell volume over the course of the multi-cycle flash sintering experiment.

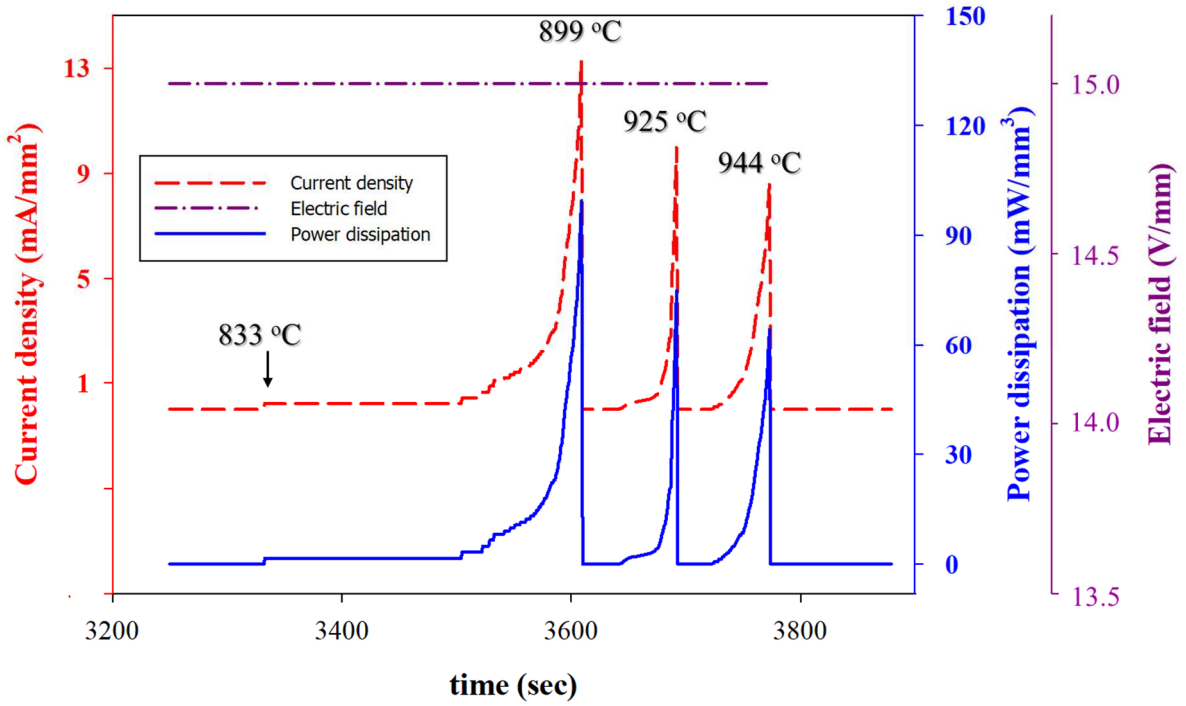

Figure 2. The variation of current density and power dissipation as a function of time under 15 V/mm during the triple-flash sintering experiment of 8% Y_2O_3 stabilized ZrO_2 in this study (heating rate is 15 °C/min and is constant).

A typical diffraction pattern of cubic 8%YSZ that was obtained in this study in shown in **Fig.3**. Such a spectrum was obtained with 2 seconds temporal resolution, resulting in the collection of over 1000 spectra from which the cubic lattice parameter and the unit cell volume was obtained as a function of time and the applied electric field as depicted in **Fig. 4**. Up to 833 °C, the 8%YSZ exhibited thermal expansion as the furnace temperature increased which is indicated by the baselines (see **Fig. 4**). Three maxima at 899, 925 and 944 °C were observed in both the cubic cell parameter and the unit cell volume that coincide with the peak power absorptions associated with the current-voltage response. The observed unit cell expansions at 899, 925 and 944 °C are 0.54%, 0.483% and 0.42%, respectively. By comparing **Figs. 2** and **4**, it is clear that the unit cell expansion is induced by the passage of

current (equivalently by the absorption of power) through 8%YSZ. We note that the magnitude of the induced unit cell expansion is proportional to the magnitude of the current draw by the sample, i.e., the lower the current draw, and the lower the unit cell expansion.

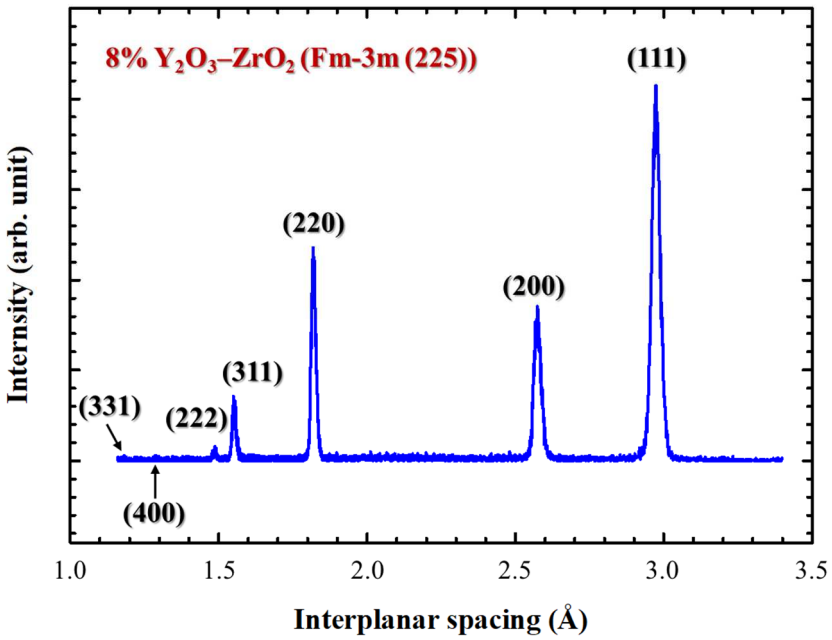

Figure 3. Representative *in situ* energy dispersive x-ray diffraction pattern of 8% Y_2O_3 stabilized ZrO_2 that was obtained over the course of the triple-flash sintering experiment under 15 V/mm electric field (heating rate is 15 ^oC/min and is constant). using a synchrotron probe with photon energies up to 200 keV. Full spectra were acquired with a 2 second temporal resolution using a polychromatic synchrotron probe with photon energies up to 200 keV.

The maximum unit cell expansion (0.54%) was observed for 13 mA/mm^2 current density which is the transient corresponding to the precipitous densification by flash sintering occurred. The relaxation of the unit cell volume upon cutting off the power at each maximum is anelastic as it exhibits time dependence and is fully recovered to the floating baseline. We attribute the floating baseline, which spans from 833 to 969 ^oC, to Joule heating which is unavoidable as discussed elsewhere[12]. The linear

baseline, on the other hand, is due to the isobaric volumetric thermal expansion[5]. However, we conjecture that the observed maxima at 899, 925 and 944 °C are the signatures of flash sintering[5, 12]. What distinguished our experiment from traditional flash sintering studies is the multicycle approach which enabled us to gain further insight. Next, we will examine the signature of defect processes on the observed x-ray data in conjunction with the observed unit cell volume anomalies.

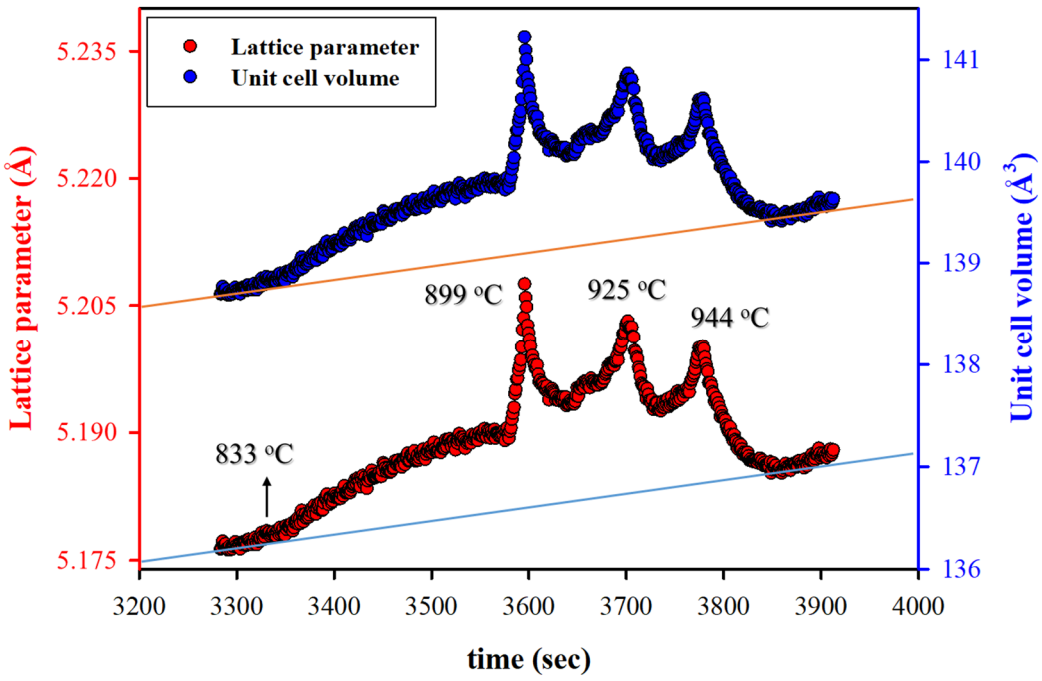

Figure 4. The variation of unit cell parameter and volume as a function of time under 15 V/mm electric field during the triple-flash sintering experiment of 8% Y_2O_3 stabilized ZrO_2 in this study (heating rate is 15 °C/min and is constant).

Figure 5 shows the variation of the full width at half maximum (FWHM) of the (111) Bragg peak (see **Fig. 3**) as a function of time under 15 V/mm during the flash sintering experiment of 8%YSZ in this study. At 899°C, a singularity was observed in the FWHM data which coincides with the singularities observed in the current-voltage response (see **Fig. 2**) and the unit cell volume data (see **Fig. 4**) which is in conformity

with what we have reported earlier [5]. Such a singularity in FWHM was attributed to the changes in the oxygen vacancy concentration and their rearrangement during stage 2 of flash sintering where identification occurs. In the experiment reported herein, we also observed small singularities in the FWHM that coincide with the second and third singularities of **Figs. 2** and **4**. As discussed earlier, the first singularity at 899 ^{o}C is associated with the precipitous densification and the formation of grain boundaries. Therefore, we attribute the large singularity in the (111) FWHM at 899 ^{o}C to defect processes governing the solid state diffusion flux responsible for densification[5]. Since solid state diffusion is governed by oxygen vacancy migration in 8YSZ, we conjecture that the changes of the (111) FHWM is due to processes involving oxygen vacancies[5, 12]. While the singularity in the (111) FHWM provides proof of defect processes associated with flash sintering, one needs to consider the following question: Does the singularity at 899 ^{o}C correlate with the creation of excess oxygen vacancies whereby the diffusivity is enhanced? In order to shed some light to this question, the variation of the integrated (111) peak area with time was analyzed (see **Fig. 6**). We observed a ~37% decrease in the integrated peak area for the 899 ^{o}C singularity, while the same for the 925 and 944 ^{o}C was negligibly small. We attribute the decrease in the (111) integrated area to the creation of excess vacancies under the action of the electric field leading to the 899 ^{o}C singularity [49]. The singularity in the (111) peak areas a 925 and 944 ^{o}C are not as pronounced as the one at 899 ^{o}C. We attribute this to the fact that the densification had already occurred, and grain boundaries had already formed.

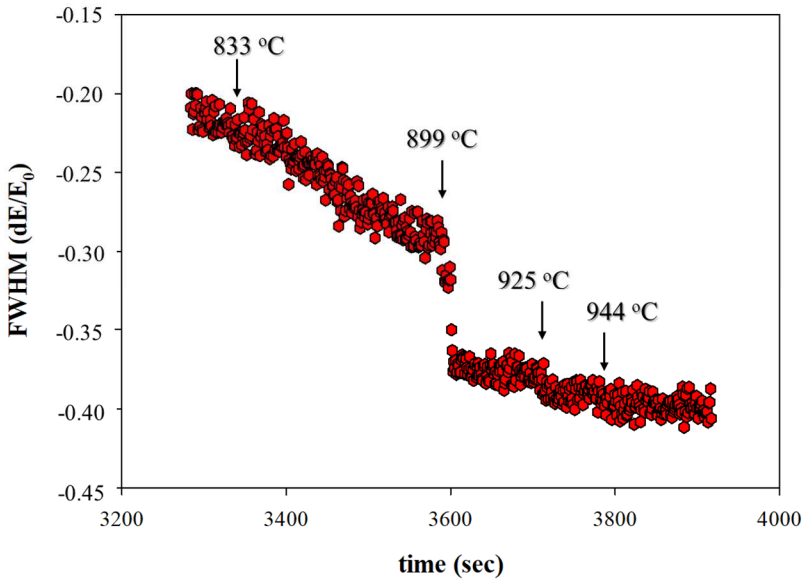

Figure 5. The variation of full width at half maximum of (111) Bragg peak as a function of time under 15 V/mm during the triple-flash sintering experiment of 8% Y_2O_3 stabilized ZrO_2 in this study (heating rate is 15 °C/min and is constant).

Above all, we note that the variation of the (111) integrated peak area is constant up to 899 °C indicating that the applied field and the temperature has no macroscopically observable effect. Over the same temperature range, the (111) FWHM exhibits a monotonic decrease up to 899 °C. While the mechanisms of the defect processes remain to be elucidated, it is clear that flash sintering is closely related to oxygen vacancy-based defect processes that appears to be interface controlled and driven by the electric field.

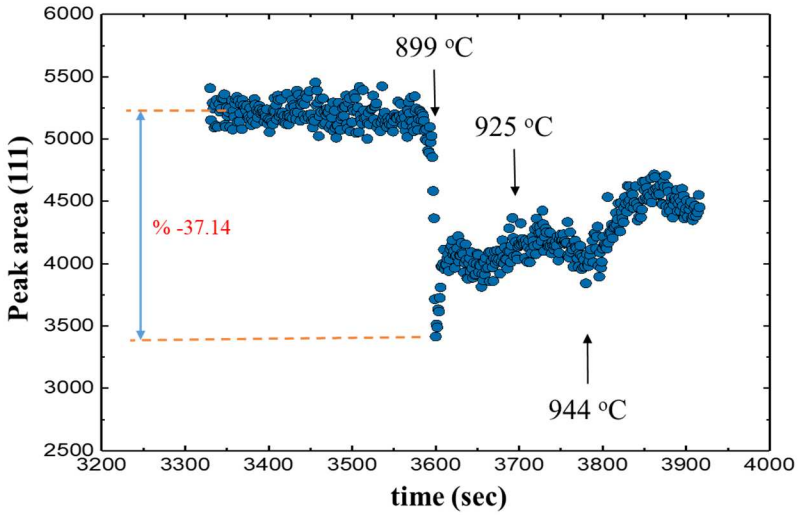

Figure 6. The variation of (111) integrated peak area as a function of time under 15 V/mm during the triple-flash sintering experiment of 8% Y_2O_3 stabilized ZrO_2 in this study (heating rate is 15 °C/min and is constant).

Figure 7 depicts the microstructure of the flash sintered 8%YSZ to 97% of the theoretical density that was obtained in this study under the aforementioned conditions. The microstructure was comprised of ~250 nm grain size, which suggested that no grain growth occurred (initial power particle size was also ~250 nm). Furthermore, one observes well-formed grain boundary triple junctions with ~120° dihedral angle [50].

However, the grain boundaries are not fully flat, suggesting a metastable configuration as compared to a polycrystalline microstructure with fully flat grain boundaries. Nevertheless, as we have shown, a 97% dense microstructure was obtained in 75 seconds at 899 °C peak temperature. We note that such ultra-fast densification is a signature of flash sintering and not that of Joule heating as conventional sintering of 8%YSZ takes please in hours at temperatures well in excess of 1200 °C. Hence, some Joule heating cannot be avoided but it is not the governing phenomenon.[12]

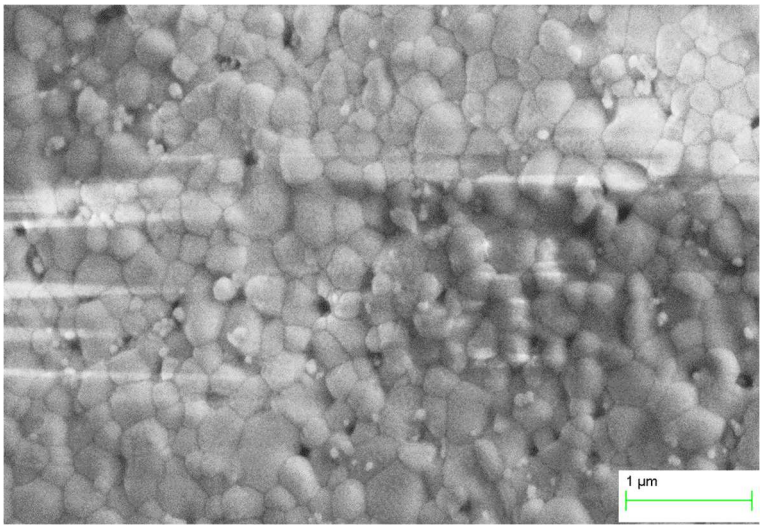

Figure 7. The microstructure of 8%YSZ after flash sintering by a triple-flash approach.

IV. Summary and Conclusion

By using in *situ* energy dispersive X-ray synchrotron diffraction, we probed the time evolution of the unit cell volume and the (111) peak width and integrated peak area with 2 seconds temporal resolution during the flash sintering of 8%YSZ. The results reveal the structural alteration in the ceramic materials during flash sintering. A thrice repeated multicycle flash sintering approach revealed that three distinct anomalies the magnitude of which decrease once precipitous densification occurred. The said multicycle approach provided additional insight to electric field induced anomalous lattice expansion and anelastic lattice relaxation under open circuit conditions, none of which is related to Joule heating. The observed anomalies are signatures of flash sintering the exact mechanisms of which remain to be unearthed.

Acknowledgement

The authors wish to thank Dr. Zhong Zhong (Brookhaven National Laboratory, Upton, NY, USA) for his valuable technical feedback. This research was accomplished in part at the National Synchrotron Light Source, a U.S. Department of Energy (DOE) Office of Science User Facility operated for the DOE Office of Science by Brookhaven National Laboratory under Contract No. DE-AC02-98CH10886.

References

1. Bordia, R. K.; Kang, S. J. L.; Olevsky, E. A., Current understanding and future research directions at the onset of the next century of sintering science and technology. *Journal of the American Ceramic Society* **2017,** *100* (6), 2314-2352.
2. Duffy, T. S.; Hemley, R. J.; Mao, H.-k., Equation of state and shear strength at multimegabar pressures: Magnesium oxide to 227 GPa. *Physical Review Letters* **1995,** *74* (8), 1371.
3. Rhodes, W. H., Agglomerate and particle size effects on sintering yttria-stabilized zirconia. *Journal of the American Ceramic Society* **1981,** *64* (1), 19-22.
4. Zhang, H.; Kim, B. N.; Morita, K.; Yoshida, H.; Lim, J. H.; Hiraga, K., Optical properties and microstructure of nanocrystalline cubic zirconia prepared by high-pressure spark plasma sintering. *Journal of the American Ceramic Society* **2011,** *94* (9), 2981-2986.
5. Akdoğan, E.; Şavklıyıldız, İ.; Biçer, H.; Paxton, W.; Toksoy, F.; Zhong, Z.; Tsakalakos, T., Anomalous lattice expansion in yttria stabilized zirconia under simultaneous applied electric and thermal fields: A time-resolved in situ energy dispersive x-ray diffractometry study with an ultrahigh energy synchrotron probe. *Journal of Applied Physics* **2013,** *113* (23), 233503.
6. Bicer, H.; Beyoglu, B.; Ozdemir, T. E.; Okasinski, J.; Tsakalakos, T., Direct in situ observation of electric field assisted densification of ZnO by energy dispersive X-ray diffraction. *Ceramics International* **2019,** *45* (6), 7614-7618.
7. Cologna, M.; Prette, A. L.; Raj, R., Flash-sintering of cubic yttria-stabilized zirconia at 750° C for possible use in SOFC manufacturing. *Journal of the American Ceramic Society* **2011,** *94* (2), 316-319.
8. Özdemir, T. E.; Akdoğan, E. K.; Şavklıyıldız, İ.; Biçer, H.; Örnek, M.; Zhong, Z.; Tsakalakos, T., Electric field effect on chemical and phase equilibria in nano-TiB2–TiO2–TiBO3 system at< 650 C: an in situ time-resolved energy dispersive x-ray diffraction study with an ultrahigh energy synchrotron probe. *Journal of Materials Research* **2017,** *32* (2), 482-494.
9. Prette, A. L.; Cologna, M.; Sglavo, V.; Raj, R., Flash-sintering of Co2MnO4 spinel for solid oxide fuel cell applications. *Journal of Power Sources* **2011,** *196* (4), 2061-2065.
10. Raj, R., Joule heating during flash-sintering. *Journal of the European Ceramic Society* **2012,** *32* (10), 2293-2301.
11. ŞAVKLIYILDIZ, İ.; DEMİR, A., Flash Sintering Effect on PMN-PT Ceramics. *El-Cezeri Journal of Science and Engineering 8* (2), 793-799.
12. Şavklıyıldız, İ.; Okur, Ç.; Akdoğan, E. K., Flash sintering and dielectric properties of K0. 5Na0. 5NbO3. *Journal of the American Ceramic Society* **2022,** *105* (1), 469-480.
13. Becker, M. Z. e.; Baltianski, S.; Popilevsky, L.; Attias, R.; Paul, T.; Tsur, Y., Flash-Sintering Mechanism Studied Through Interrupted Experiments. *Advanced Engineering Materials* **2021,** *23* (7), 2001499.
14. Cologna, M.; Rashkova, B.; Raj, R., Flash sintering of nanograin zirconia in< 5 s at 850 C. *Journal of the American Ceramic Society* **2010,** *93* (11), 3556-3559.
15. Jha, S. K.; Charalambous, H.; Wang, H.; Phuah, X. L.; Mead, C.; Okasinski, J.; Wang, H.; Tsakalakos, T., In-situ observation of oxygen mobility and abnormal lattice expansion in ceria during flash sintering. *Ceramics International* **2018,** *44* (13), 15362-15369.
16. Karakuscu, A.; Cologna, M.; Yarotski, D.; Won, J.; Francis, J. S.; Raj, R.; Uberuaga, B. P., Defect structure of flash-sintered strontium titanate. *Journal of the American Ceramic Society* **2012,** *95* (8), 2531-2536.
17. M'Peko, J.-C.; Francis, J. S.; Raj, R., Field-assisted sintering of undoped BaTiO3: Microstructure evolution and dielectric permittivity. *Journal of the European Ceramic Society* **2014,** *34* (15), 3655-3660.

18. Biesuz, M.; Pinter, L.; Saunders, T.; Reece, M.; Binner, J.; Sglavo, V. M.; Grasso, S., Investigation of electrochemical, optical and thermal effects during flash sintering of 8YSZ. *Materials* **2018,** *11* (7), 1214.
19. Castro, R.; Van Benthem, K., *Sintering: mechanisms of convention nanodensification and field assisted processes*. Springer Science & Business Media: 2012; Vol. 35.
20. Cologna, M.; Francis, J. S.; Raj, R., Field assisted and flash sintering of alumina and its relationship to conductivity and MgO-doping. *Journal of the European Ceramic Society* **2011,** *31* (15), 2827-2837.
21. Todd, R.; Zapata-Solvas, E.; Bonilla, R.; Sneddon, T.; Wilshaw, P., Electrical characteristics of flash sintering: thermal runaway of Joule heating. *Journal of the European Ceramic Society* **2015,** *35* (6), 1865-1877.
22. Glicksman, M., Diffusion in solids: field theory, solid-state principles, and applications. *New York* **2000**, 54-56.
23. Goff, J.; Hayes, W.; Hull, S.; Hutchings, M.; Clausen, K. N., Defect structure of yttria-stabilized zirconia and its influence on the ionic conductivity at elevated temperatures. *Physical Review B* **1999,** *59* (22), 14202.
24. Guo, X.; Ding, Y., Grain boundary space charge effect in zirconia: Experimental evidence. *Journal of the Electrochemical Society* **2003,** *151* (1), J1.
25. Maier, J., Nanoionics: ionic charge carriers in small systems. *Physical Chemistry Chemical Physics* **2009,** *11* (17), 3011-3022.
26. Park, H. J.; Choa, Y. H., The grain boundary conduction property of highly dense and nanostructured yttrium-doped zirconia. *Electrochemical and Solid-State Letters* **2010,** *13* (5), K49.
27. Shewmon, P., *Diffusion in solids*. Springer: 2016.
28. Guo, X., Can we achieve significantly higher ionic conductivity in nanostructured zirconia? *Scripta Materialia* **2011,** *65* (2), 96-101.
29. Dong, Y.; Chen, I. W., Onset criterion for flash sintering. *Journal of the American Ceramic Society* **2015,** *98* (12), 3624-3627.
30. Du, Y.; Stevenson, A. J.; Vernat, D.; Diaz, M.; Marinha, D., Estimating Joule heating and ionic conductivity during flash sintering of 8YSZ. *Journal of the European Ceramic Society* **2016,** *36* (3), 749-759.
31. Francis, J. S.; Raj, R., Influence of the field and the current limit on flash sintering at isothermal furnace temperatures. *Journal of the American Ceramic Society* **2013,** *96* (9), 2754-2758.
32. Ghosh, S.; Chokshi, A. H.; Lee, P.; Raj, R., A huge effect of weak dc electrical fields on grain growth in zirconia. *Journal of the American Ceramic Society* **2009,** *92* (8), 1856-1859.
33. Hao, X.; Liu, Y.; Wang, Z.; Qiao, J.; Sun, K., A novel sintering method to obtain fully dense gadolinia doped ceria by applying a direct current. *Journal of Power Sources* **2012,** *210*, 86-91.
34. Raj, R.; Cologna, M.; Francis, J. S., Influence of externally imposed and internally generated electrical fields on grain growth, diffusional creep, sintering and related phenomena in ceramics. *Journal of the American Ceramic Society* **2011,** *94* (7), 1941-1965.
35. Chaim, R., Particle surface softening as universal behaviour during flash sintering of oxide nano-powders. *Materials* **2017,** *10* (2), 179.
36. M'Peko, J. C.; Francis, J.; Raj, R., Impedance spectroscopy and dielectric properties of flash versus conventionally sintered yttria-doped zirconia electroceramics viewed at the microstructural level. *Journal of the American Ceramic Society* **2013,** *96* (12), 3760-3767.
37. Şavklıyıldız, İ., Thermal equation of state study of polymorphic phases of Y2O3. *Journal of Applied Physics* **2021,** *129* (8), 085108.
38. Biçer, H.; Akdoğan, E. K.; Şavklıyıldız, İ.; Haines, C.; Zhong, Z.; Tsakalakos, T., Thermal expansion of nano–boron carbide under constant DC electric field: An in situ energy dispersive X-ray diffraction study using a synchrotron probe. *Journal of Materials Research* **2020,** *35* (1), 90-97.
39. Akdoğan, E.; Şavklıyıldız, İ.; Berke, B.; Zhong, Z.; Wang, L.; Vaughan, M.; Tsakalakos, T., High-pressure phase transformations in MgO-Y2O3 nanocomposites. *Applied Physics Letters* **2011,** *99* (14), 141915.

40. Akdoğan, E.; Şavklıyıldız, İ.; Berke, B.; Zhong, Z.; Wang, L.; Weidner, D.; Croft, M.; Tsakalakos, T., Pressure effects on phase equilibria and solid solubility in MgO-Y2O3 nanocomposites. *Journal of Applied Physics* **2012,** *111* (5), 053506.
41. ŞAVKLIYILDIZ, İ., In-Situ Strain Measurement on Al7075 Plate by Using High Energy Synchrotron Light Source. *Avrupa Bilim ve Teknoloji Dergisi* (23), 435-439.
42. Şavklıyıldız, İ.; Akdoğan, E.; Zhong, Z.; Wang, L.; Weidner, D.; Vaughan, M.; Croft, M.; Tsakalakos, T., Phase transformations in hypereutectic MgO-Y2O3 nanocomposites at 5.5 GPa. *Journal of Applied Physics* **2013,** *113* (20), 203520.
43. Simos, N.; Elbakhshwan, M.; Zhong, Z.; Ghose, S.; Savkliyildiz, I., High-temperature annealing of proton irradiated beryllium–A dilatometry-based study. *Journal of Nuclear Materials* **2016,** *477*, 1-17.
44. Simos, N.; Zhong, Z.; Dooryhee, E.; Ghose, S.; Gill, S.; Camino, F.; Şavklıyıldız, İ.; Akdoğan, E., Neutron irradiation and high temperature effects on amorphous Fe-based nano-coatings on steel–A macroscopic assessment. *Journal of Nuclear Materials* **2017,** *489*, 164-179.
45. Paxton, W. A.; Özdemir, T. E.; Şavklıyıldız, İ.; Whalen, T.; Biçer, H.; Akdoğan, E. K.; Zhong, Z.; Tsakalakos, T., Anisotropic thermal expansion of zirconium diboride: an energy-dispersive X-ray diffraction study. *Journal of Ceramics* **2016,** *2016*.
46. Paxton, W. A.; Akdoğan, E. K.; Şavkliyildiz, I.; Choksi, A. U.; Silver, S. X.; Tsakalakos, T.; Zhong, Z., Asynchronous stoichiometric response in lithium iron phosphate batteries. *Journal of Materials Research* **2015,** *30* (3), 417-423.
47. Simos, N.; Zhong, Z.; Zhong, H.; Camino, F.; Dooryhee, E.; Ghose, S.; Sprouster, D.; Kotsina, Z.; Savkliyildiz, I.; Akdogan, E., Fast Neutron Irradiation Embrittlement-ductilitization of an Iron-based Amorphous Alloy using In Situ Synchrotron X-ray Diffraction. International Journal of Metallurgy and Metal Physics 2022, 5 (BNL-222728-2022-JAAM).
48. Holland, T.J.B.; Redfern, S.A.T., UNITCELL: a nonlinear least-squares program for cell parameter refinement implementing regression and deletion diagnostics. J. Appl. Cryst. 1997, 30, 84.
49. Li, J.; Cho, J.; Ding, J.; Charalambous, H.; Xue, S.; Wang, H.; Phuah, X. L.; Jian, J.; Wang, X.; Ophus, C., Nanoscale stacking fault–assisted room temperature plasticity in flash-sintered TiO2. Science advances 2019, 5 (9), eaaw5519.
50. Şavklıyıldız,I; Okur, Ç.; Akdoğan, E.K., Flash sintering and dielectric properties of K0.5Na0.5NbO3. Journal of American Ceramic Society, 2022, 105, 469–480.

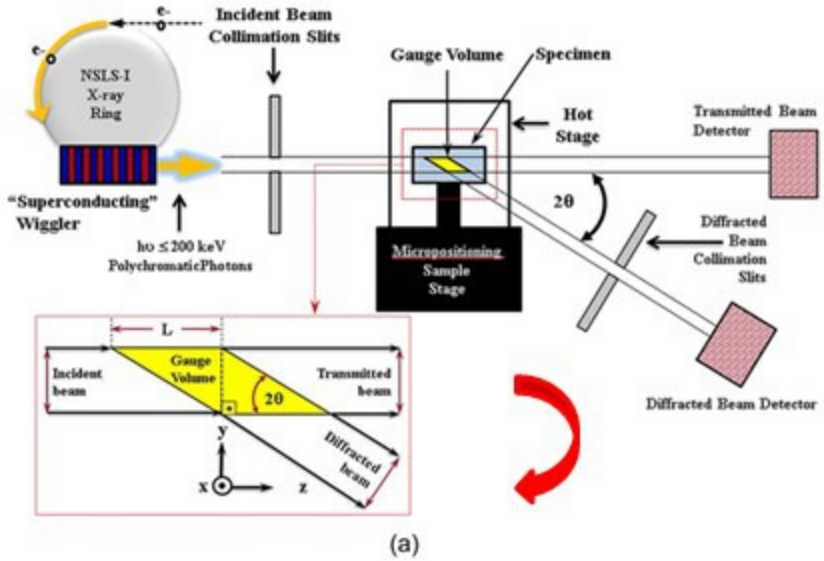
e-
e-
Incident Beam
Collimation Slits
NSLS-I
X-ray
Ring
Gauge Volume
Specimen
Hot
Stage
Transmitted Beam
Detector
"Superconducting"
Wiggler
hυ ≤ 200 keV
PolychromaticPhotons
2θ
Diffracted
Beam
Collimation
Slits
Micropositioning
Sample
Stage
Diffracted Beam Detector
L
Incident
beam
Gauge
Volume
2θ
Transmitted
beam
Diffracted
beam
y
x
z

(a)

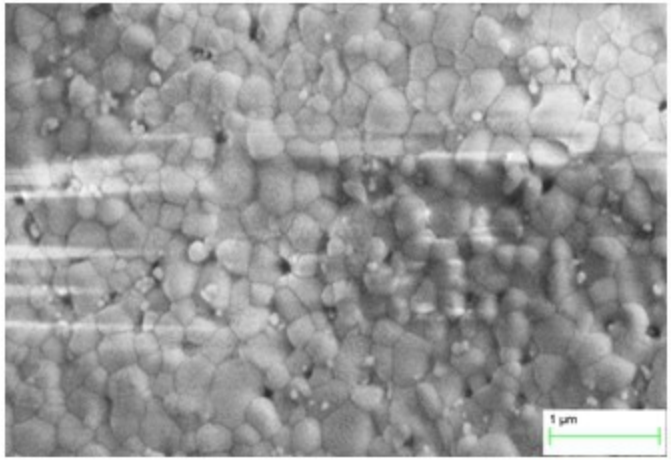
1 μm

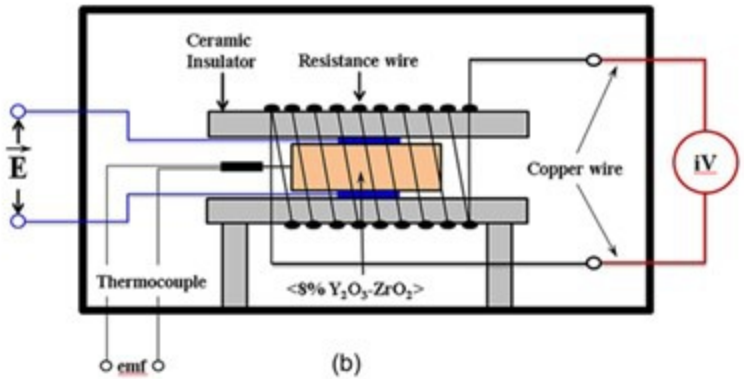
Ceramic
Insulator
Resistance wire
E
Copper wire
iV
Thermocouple
<8% Y2O3-ZrO2>
emf

(b)

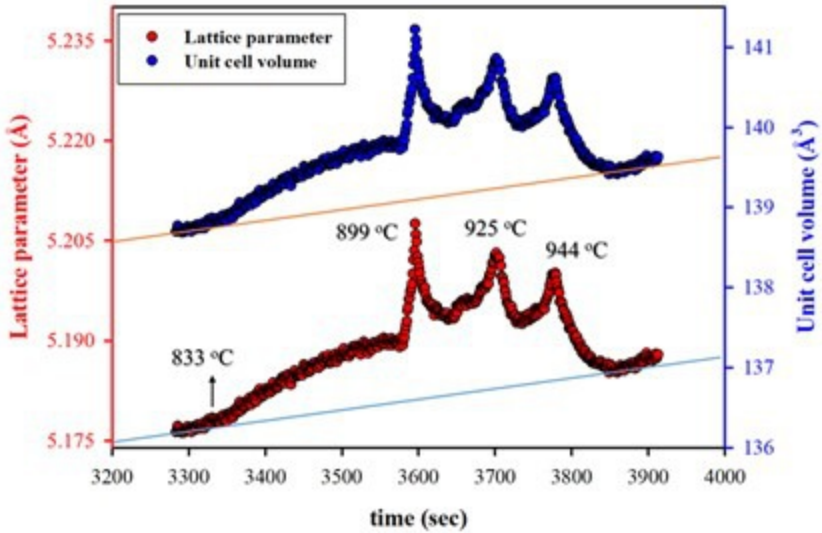
Lattice parameter
Unit cell volume
Lattice parameter (Å)
Unit cell volume (Å³)
5.235
5.220
5.205
5.190
5.175
141
140
139
138
137
136
899 °C
925 °C
944 °C
833 °C
3200
3300
3400
3500
3600
3700
3800
3900
4000
time (sec)